Digital Object Identifier 10.1109/CPE-POWERENG50821.2021.9501085

2021 IEEE 15th International Conference on Compatibility, Power Electronics and Power Engineering (CPE-POWERENG)

Multiwinding Transformer Leakage Inductance Optimization for Power Flow Decoupling in Multiport DC-DC Converters

Hamzeh Beiranvand
Felix Hoffmann
Yoann Pascal
Frederik Hahn
Marco Liserre

Suggested Citation

H. Beiranvand, F. Hoffmann, Y. Pascal, F. Hahn and M. Liserre, "Multiwinding Transformer Leakage Inductance Optimization for Power Flow Decoupling in Multiport DC-DC Converters," 2021 IEEE 15th International Conference on Compatibility, Power Electronics and Power Engineering (CPE-POWERENG), 2021.

Multiwinding Transformer Leakage Inductance Optimization for Power Flow Decoupling in Multiport DC-DC Converters

Hamzeh Beiranvand
Chair of Power Electronics
Kiel University
Kiel, Germany
hab@tf.uni-kiel.de

Felix Hoffmann
Chair of Power Electronics
Kiel University
Kiel, Germany
fho@tf.uni-kiel.de

Yoann Pascal
Chair of Power Electronics
Kiel University
Kiel, Germany
yopa@tf.uni-kiel.de

Frederik Hahn
Chair of Power Electronics
Kiel University
Kiel, Germany
frha@tf.uni-kiel.de

Marco Liserre
Chair of Power Electronics
Kiel University
Kiel, Germany
ml@tf.uni-kiel.de

***Abstract*—Isolated multiport DC-DC converters manifest some prominent advantages over usual multiple two-port DC-DC converters such as smaller holistic magnetics and higher power density. However, the operation of such a converter is tied to the power flow decoupling capability in the magnetic medium frequency transformer (MFT). This paper targets to optimize the decoupling between the multiwinding MFT ports by means of multi-objective optimization of the leakage inductance network. Three different multi-objective cost functions are proposed and solved by Genetic Algorithm (GA). The obtained results show that a winding topology where primary winding is sandwiched by the two secondaries and are tightly wound to the core, provides the minimum possible leakage inductance without interleaving the windings. The obtained topologies from solving different objectives can be used as a benchmark in design and manufacturing of mutliwinding transformers. Experimental results are provided to verify the obtained optimum design.**

***Index Terms*—Multiwinding MFT, Isolated Multiport DC-DC Converters, Power Flow Decoupling, Inductance Network, Genetic Algorithm**

I. Introduction

Isolation is inevitable in many DC-DC applications such as EV charging and sensitive data centers to provide safety, efficiency, level shifting and avoiding noisy ground currents. Multiwinding MFTs are one of the most promising solutions in multiport isolated DC-DC converters.

Converter topologies employing multiwinding MFTs have been the subject of many research works in the last decades. In [1], the voltage of the cascaded H-bridge converter (CHB) cells is balanced using the power management capabilities of the multiwinding MFT. In [2], the multiwinding MFT has been applied to the power electronic transformer for traction applications. Photovoltaic array integration into CHB cells has been demonstrated in [3]. The multiwinding MFTs have been utilized in battery energy storage systems as in [4] and [5]. Other applications such as energy routing ability of multiwinding MFT [6], electric aircraft [7], medium voltage (MV) distribution [8] and smart transformers [9], [10] could be added to this literature. Multiwinding MFTs sought to be an economic and flexible galvanic isolation interface for many emerging applications, however, the problem of cross-coupling between the multiwinding MFT ports imposes complexity on the independent operation of the multiport DC-DC converters.

The power flow decoupling between the ports has been reported in two ways. First method is to use control techniques in the software of the controller by a lookup table [11]. This method is not scalable and impose complexity on the design of the controller. The second way decouples the power from the root of the problem, i.e. the inductance network of the multiwinding transformer as in [12]. The method can decrease the controller implementation complexity greatly. However, the design methodology for achieving required inductance network has not been developed proportionally.

Analytical calculation of the leakage inductance has been the focus of numerous research works [13], [14], [15]. Whereas, there are few works that are dealing with the design of multiwinding transformers [16]. Leakage inductance of a conventional two-winding MFT has been optimized in [17] where the leakage energy of the transformer is minimized by tuning the inter-winding distance and inter-turn distance of the secondary winding. The leakage inductance optimization of two-winding MFT is straight forward in comparison with the

This work was carried out in the BAEW project funded by the WTSH and the EKSH of Schleswig-Holstein (LPW-E/1.1.2/1486).

978-1-7281-8071-7/21/$31.00

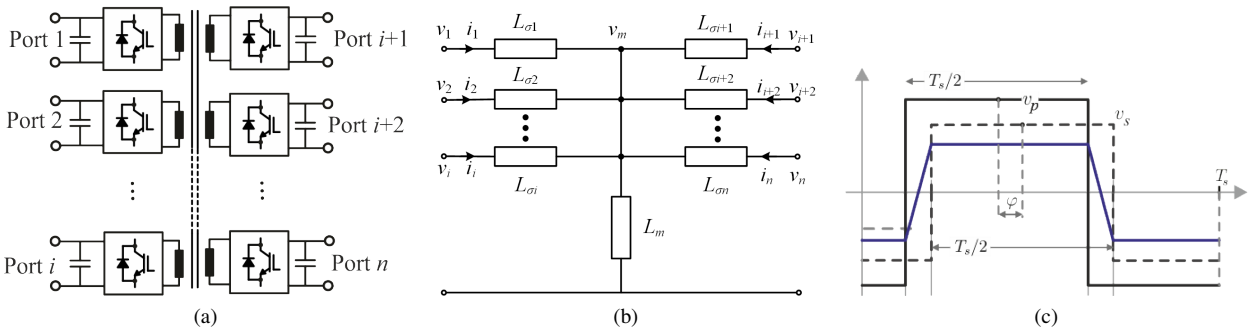

Fig. 1. Multiport isolated DC-DC converter: (a) Generalized Multiport DC-DC converter; (b) Multi-winding transformer utilized as the isolation stage and (c) basic DAB converter current (blue) and voltage (black) waveforms operated with phase shift modulation (PM).

multiwinding transformer because the challenge of the cross-coupling of the ports does not exist in the two-winding MFT.

The main contribution of this paper is to optimize the design of the inductance network of the multiwinding MFTs in order to overcome the cross-coupling problem between the ports. Initially, the theoretical background of the inductance network cross-coupling is demonstrated and the basis for inductance optimization is formed. Consequently, double Fourier series (DFS) method is extended for the calculation of multiwinding transformer leakage inductances. DFS connects the winding geometry and configuration to the inductance magnitudes and therefore it is used in multi-objective optimization problems. The optimization problems are solved by GA and the derived results are analyzed and verified by FEM simulation. The design examples and the experimental results provide a clear insight into the multiwinding transformer design for cross-coupling suppression in multiport DC-DC converters.

II. Leakage Inductance Network Requirements

The operation of a multiport converter is a function of the multiwinding MFT leakage inductance network. In the following, the power flow analysis and inductance requirements are described.

A. Power Flow Analysis

A generalized multiport DC-DC converter topology is shown in Fig. 1 (a). The operation of DC-DC converter is controlled by the impedance network of the multiwinding MFT. In the following, power flow capabilities of the multiwinding MFT is evaluated. Fig. 1 (b) shows the equivalent circuit of the multiwinding MFT. Voltage and current waveforms of the transformer are assumed pure sinusoid at steady-state. Utilizing voltage phasor for ports, i.e. $v_i = V_i e^{j\theta_i}$, fictitious magnetizing voltage can be defined as:

$$v_m = L_{eq} \sum_{n=1}^{n} \frac{v_i}{L_i} \quad \text{where} \quad \frac{1}{L_{eq}} = \frac{1}{L_m} + \sum_{n=1}^{n} \frac{1}{L_i} \tag{1}$$

where L_m and L_i are, respectively, the magnetizing inductance and the leakage inductance of winding i, whereas v_m and v_i are, respectively, the voltage at the nodes in Fig. 1 (b). Fictitious magnetizing voltage determines the power flow capability of each port depending on the operating point of the other ports. Considering power flow at port i:

$$S_i = v_i \left(\frac{v_i - v_m}{j\omega L_i} \right)^* = v_i \left(\frac{v_i - L_{eq} \sum_{k=1}^{n} \frac{v_k}{L_k}}{j\omega L_i} \right)^* \tag{2}$$

The complex injected power at port i can be derived simply:

$$\begin{aligned} S_i &= \frac{v_i v_i^*}{-j\omega L_i} - \frac{L_{eq}}{-j\omega L_i} \sum_{k=1}^{n} \frac{v_i v_k^*}{L_k} \\ &= \frac{V_i^2}{-j\omega L_i} \left(1 - \frac{L_{eq}}{L_i} \right) - \frac{L_{eq}}{-j\omega L_i} \sum_{k=1, k\neq i}^{n} \frac{v_i v_k^*}{L_k} \end{aligned} \tag{3}$$

Finally, active and reactive power flow equations can be stated as:

$$P_i = \Re(S_i) = \frac{L_{eq}}{\omega L_i} \sum_{k=1, k\neq i}^{n} \frac{V_i V_k \sin(\theta_i - \theta_k)}{L_k} \tag{4}$$

and

$$Q_i = \frac{V_i^2}{\omega L_i} \left(1 - \frac{L_{eq}}{L_i} \right) - \frac{L_{eq}}{\omega L_i} \sum_{k=1, k\neq i}^{n} \frac{V_i V_k \cos(\theta_i - \theta_k)}{L_k} \tag{5}$$

As a result, the power flow between port i and k is:

$$P_{ik} = \frac{L_{eq}}{\omega L_i L_k} V_i V_k \sin(\theta_i - \theta_k) \tag{6}$$

If $L_i \to 0$ then $L_{eq} \to 0$ and $v_m \approx V_i$ which implies v_m can be fixed by connecting it to a voltage source. Moreover, power flow between port i and k reduces to:

$$P_k = P_{ik} = \frac{V_i V_k}{\omega L_k} \sin(\theta_i - \theta_k) \tag{7}$$

which implies that the power flow of port k only depends on its leakage inductance L_k. Hence the power flow between the other ports can be decoupled as stated in [12]. Even-though it is possible to achieve any value for L_i in theory, however, due to design and manufacturing uncertainties it is impossible to achieve this objective perfectly.

B. Inductance Determination

For a given set of the voltage ratings, power flow control is limited to the design of leakage inductances and power angle differences between each two ports. In a conventional two-port DAB converter, voltage and current waveforms are shown in Fig. 1 (c). In the case of nonsinusoidal voltage and current waveforms, Fourier series can be used and this equation can be developed for the respective frequencies. For this special case where currents have a trapezoidal shape, average active power flow can be written as:

$$P_{DAB} = \frac{V_p V_s}{\omega L_\sigma} \varphi \left(1 - \frac{\varphi}{\pi}\right) \tag{8}$$

In a multiport configuration the assumption of trapezoidal currents can not be hold anymore. Because, the magnetic coupling between the windings influences on the current waveform. In general, Fourier transform of the voltage can be used to do a comprehensive analysis in the phasor domain at each frequency. Fourier series for two voltage waveforms with zero phase angle and φ are given in the following:

$$v_p(t) = \sum_{n=1,3,\dots}^{\infty} \frac{4V_p}{n\pi} \sin(n\omega t) \tag{9}$$

$$v_s(t) = \sum_{n=1,3,\dots}^{\infty} \frac{4V_s}{n\pi} \sin(n\omega t - n\varphi) \tag{10}$$

Considering the orthogonality between frequencies, the power flow at each frequency can be carried out, separately. For the harmonic number n, apparent power can be calculated as:

$$\begin{aligned} S &= \frac{1}{2} \sum_{n=1,3,\dots}^{\infty} V_{pn} \times I_n^* \\ &= \frac{1}{2} \sum_{n=1,3,\dots}^{\infty} V_{pn} \times \left(\frac{V_p - V_s e^{-jn\varphi}}{jn\omega L}\right)^* \end{aligned} \tag{11}$$

then active and reactive power flows (P_n and Q_n) from primary port for harmonic n are:

$$P_n = \frac{16 V_{pn} V_{sn}}{2(n\pi)^2 n\omega L} sin(n\varphi) \tag{12}$$

$$Q_n = \frac{16 V_{pn}^2}{(n\pi)^2 n\omega L} - \frac{16 V_{pn} V_{sn}}{2(n\pi)^2 n\omega L} cos(n\varphi) \tag{13}$$

this could be interpreted as a circle:

$$P_n^2 + \left(Q_n - \frac{16 V_{pn}^2}{2(n\pi)^2 n\omega L}\right)^2 = \left(\frac{16 V_{pn} V_{sn}}{2(n\pi)^2 n\omega L}\right)^2 \tag{14}$$

Fig. 2 (a) shows the relationship between the (P, Q) powers and φ assuming that the power is conveyed only by the fundamental using (12) and (13) with n=1 or using the full spectrum over $n \in \{1, 3, ..., 1000\}$ for an example 10kV and 400V DAB converter. Similarly, Fig. 2 (b) shows the (PQ) plane calculated using (14) with n=1 or the full spectra which resembles the DAB converter with square waveforms (blue). A small difference arises, but the first order approximation already provides a sound estimate of the power transfers. Therefore, both equations (7) and (8) can be used to specify the required leakage inductance. Using (8)

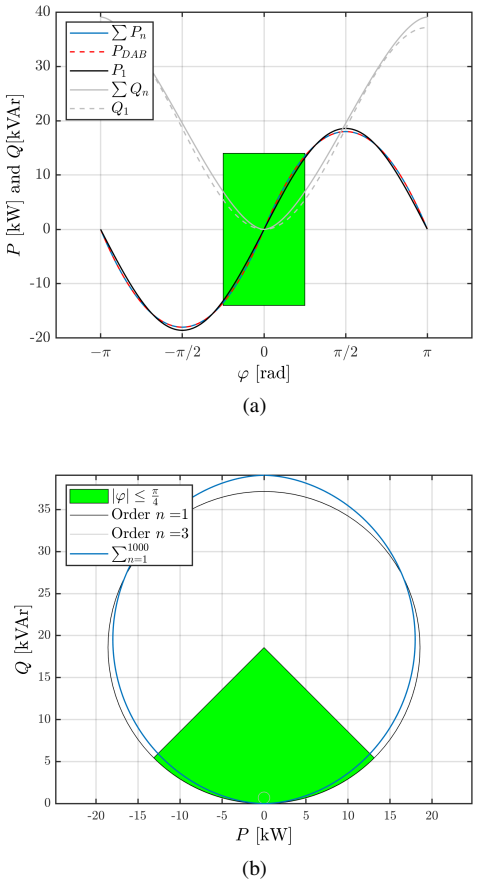

Fig. 2. DAB converter operation: (a) active and reactive power versus phase-shift angle and (b) P-Q plane

$$L_{SP,k} = \frac{V_p V_s}{\omega P_{N,k}} \varphi_{N,k} \left(1 - \frac{\varphi_{N,k}}{\pi}\right) \tag{15}$$

where $\varphi_{N,k}$ and $P_{N,k}$ are the nominal phase-shift and power of port k in the same order.

III. Leakage Inductance Optimization Methodology

In applications such as solid-state transformers, owing to circuit configuration (i.e. input-series output-parallel (ISOP) and input-parallel output-parallel (IPOP)), the output port angles are mainly equal and power flow between the ports is decoupled by the modulation. However, in some application where independent operation of ports are of interest, such as triple active bridge (TAB) [11], the decoupling between the ports shall be guaranteed. Hereafter in this paper, the focus of the optimizations is on TAB converter power flow decoupling.

A. Leakage inductance modeling

Considering the self-leakage inductances in Fig. 1 (b), L_i can be calculated for a three-winding transformer as:

$$L_{\sigma 1} = \frac{1}{2}\left[L_{\sigma 12} + L_{\sigma 13} - \left(\frac{N_1}{N_2}\right)^2 L_{\sigma 23}\right] \tag{16}$$

$$L_{\sigma 2} = \frac{1}{2}\left[\left(\frac{N_2}{N_1}\right)^2 L_{\sigma 12} - \left(\frac{N_2}{N_1}\right)^2 L_{\sigma 13} + L_{\sigma 23}\right] \tag{17}$$

$$L_{\sigma 3} = \frac{1}{2}\left[-\left(\frac{N_3}{N_1}\right)^2 L_{\sigma 12} + \left(\frac{N_3}{N_1}\right)^2 L_{\sigma 13} + \left(\frac{N_3}{N_2}\right)^2 L_{\sigma 23}\right] \tag{18}$$

where $L_{\sigma ij}$ are the measured leakage inductance from short-circuit tests between windings i and j as shown in Fig. 3.

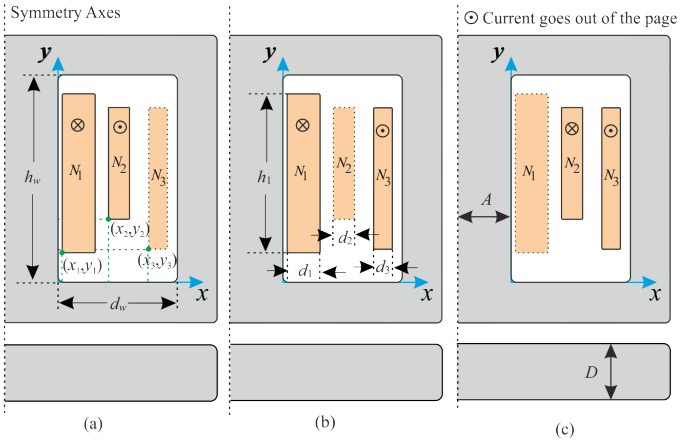

Fig. 3. Leakage inductance calculation concept: (a) measuring $L_{\sigma 12}$ while winding 1 is excited, winding 2 is shorted and winding 3 is open circuit, (b) measuring $L_{\sigma 13}$ while winding 1 is excited, winding 3 is shorted and winding 2 is open circuit and (c) measuring $L_{\sigma 23}$ while winding 2 is excited, winding 3 is shorted and winding 1 is open circuit.

Therefore, the leakage inductance calculation can be obtained similar to a conventional two-winding transformer. The stored magnetic energy per unit length of the winding in the core window can be used to calculate the leakage of each pair of windings. Then multiplying by the average magnetic length final leakage inductance is obtained. In this paper, the magnetic length is defined as the average length of the pair of windings as:

$$L_{m,ij} = 4A + 2n_c D + 4(x_i + d_i + x_j + d_j) \tag{19}$$

where A is the core yoke width and D is the core thickness. The per unit length leakage inductance is calculated using the method of double Fourier series as presented in [18].

In this publication valid under the 2D planar symmetry, assuming that the core permeability is infinite, and for an arbitrary number of windings with rectangular cross-sections, the author first expresses the current profile in the winding area using 2-dimensionnal space Fourier transform:

$$i(\theta_x, \theta_y) = \sum_{m,n} I_{mn} \cdot cos(m\theta_x) \cdot cos(n\theta_y) \tag{20}$$

where (θ_x, θ_y) are the normalised coordinates of a point in the winding window and I_{mn} are the Fourier coefficients. The space harmonics of the current I_{mn} are then used together with the local Ampère law to calculate the magnetic flux harmonics, which have a similar form as the current harmonics. These are used to derive the voltage e_{mn} induced in the winding using Faraday's law. The reactive power for the leakage inductance of each winding is then estimated by summing over the space harmonics and integrating the local power density over the volume of the winding window. The leakage reactance, and as a result the leakage inductance, can then be derived.

B. Optimization problem statement

First step in an optimization problem is to construct the objective function. The main aim of the paper is to deal with the leakage inductance optimization. Self-leakage inductance of each port might have positive, negative or zero value which has no physical interpretation. This is happening because of the considered Y equivalent circuit. In contrary, leakage inductance which is measured from short-circuit test are physically meaningful and are always positive. These values can be directly adopted in the definition of the objective functions. Depending on the nature of the application, following objectives are possible for a three winding transformer. Objective J_1 is used for minimizing the total leakage inductance.

$$J_1(u) = \begin{cases} min & f_1 = L_{\sigma 12} \\ min & f_2 = L_{\sigma 13} \\ min & f_3 = L_{\sigma 23} \end{cases} \tag{21}$$

where $u = [x_i, y_i, d_i]$ and $i \in \{1, 2, 3\}$ is the vector of control variables. Objective J_2 maximizes the total leakage inductance.

$$J_2(u) = \begin{cases} min & f_1 = \frac{1}{L_{\sigma 12}} \\ min & f_2 = \frac{1}{L_{\sigma 13}} \\ min & f_3 = \frac{1}{L_{\sigma 23}} \end{cases} \tag{22}$$

Objective J_3 maximizes the decoupling between windings 2 and 3, and maximizes the coupling between windings 1 and 2 and windings 1 and 3.

$$J_3(u) = \begin{cases} min & f_1 = L_{\sigma 12} \\ min & f_2 = L_{\sigma 13} \\ min & f_3 = \frac{1}{L_{\sigma 23}} \end{cases} \tag{23}$$

Inequality constraints include the geometrical constraints where windings may not have overlap. Moreover, the winding must situate inside the core window, i.e.

$$\begin{cases} x_i + d_i \leq d_w \\ y_i + h_i \leq h_w \\ \forall i \in \{1, 2, 3\} \end{cases} \tag{24}$$

NSGA-II [19] is adopted in this study to solve the proposed objective functions. To simplify the MFT design procedure, the constraints of the litz wires are omitted from the NSGA-II

TABLE I
SIMULATION SPECIFICATIONS

Terminal voltage 1	$V_{dc1} = 400$ V
Terminal voltage 2	$V_{dc2} = 400$ V
Terminal voltage 2	$V_{dc3} = 400$ V
MFT Ports Nominal Power	$P_{N,k}$ = 5 kW
Switching frequency	$f_s = 20$ kHz
Nominal Phase-shift angle	$\varphi_{N,k} = 30°$
Nominal Port Inductance	$L_{SP,k} = 110\mu$H
Transformer turns ratio	$n = 1$

optimization. A post optimization selection strategy is chosen for litz wires based on the methodology given in [20].

Considering a current density (J_{rms}) in the design, which can be a control variable or prespecified, the required copper area is obtained:

$$A_{Cu} = \frac{I_{rms}}{J_{rms}} \tag{25}$$

where I_{rms} is the transformer rms current and it can be calculated as in [21]. J_{rms} is the current density which can be considered as a design parameter or specify it directly. In this paper, $J_{rms} = 2$ A/mm^2 assumed.

The main design equation of the transformer is the Faraday's law of induction, where suitable number of turns can be calculated for a given core (or parallel cores) as:

$$N_i = \frac{V_{dc,i}}{4n_p A_c f_s B_m} \tag{26}$$

where $V_{dc,i}$ is the dc voltage of port i, f_s is the switching frequency, n_p is the number of parallel cores, and B_m is the flux density. Final winding area can be defined now:

$$A_{w,i} = \frac{N_i A_{Cu}}{k_f} \tag{27}$$

where k_f (=0.65 in this paper) is the filling factor of the litz wire. As the winding width d_i is a control variable then the winding height is $h_i = A_{wi}/d_i$. Core dimensions are determined based on the manufactures datasheets. Flowchart of the optimization procedure is shown in Fig. 4.

IV. DESIGN EXAMPLES

The three-winding MFT is optimized for the mentioned objectives in the previous section. Specifications of the MFT are given in Table I. Multi-objective GA with the population and generation size of 500, crossover fraction 0.8 and Pareto fraction 0.35 is configured of described objective functions J_1, J_2 and J_3. To reduce the optimization problem size and simplify the understanding of the leakage inductance variation with the winding configuration, only E100/64/28 ferrite (relative permeability $\mu_r = 1000$) cores without paralleling them are employed. Magnetic flux peak is set to $B_m = 0.3$T. Based on the considered assumptions and the specifications number of turns are $N_1 = N_2 = N_3 = 22$. The Pareto optimum faces obtained from GA are depicted in Fig. 5.

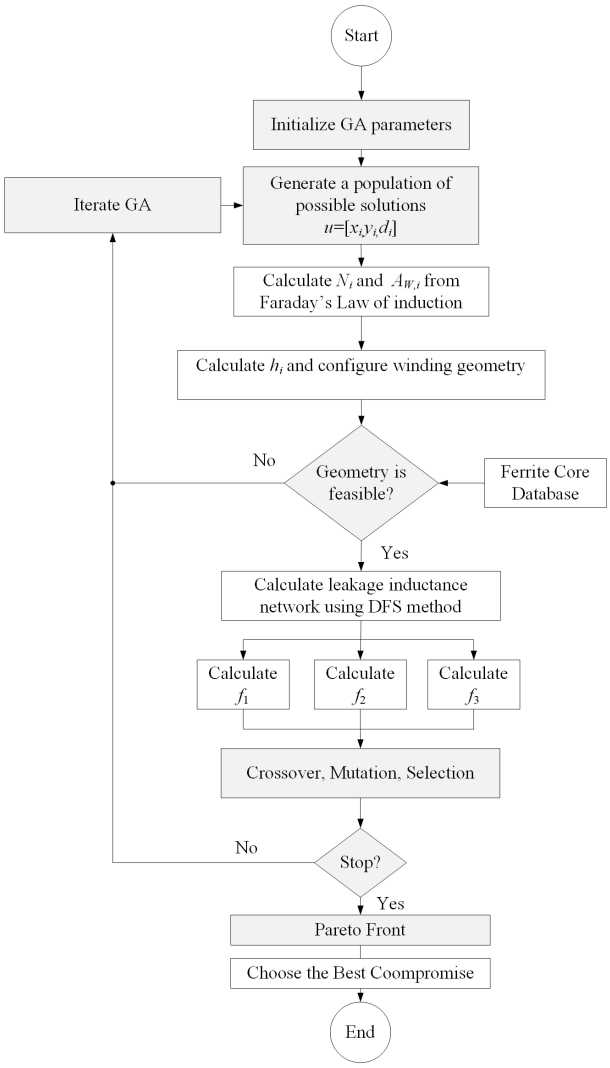

Fig. 4. Multi-objective optimization flowchart

A. J_1 optimization

Fig. 5 (a) shows the Pareto front of the objective function J_1 where all the leakage inductances are minimized. Due to the geometry limitation, it is impossible to reduce all leakage inductances to their minimum possible values. The final optimum solution shall be derived from the Pareto face based on the application requirements. In the current application, the symmetric inductance structure with maximum decoupling between output ports (ports 2 and 3) is of interest. Therefore, possible minimum value of L_{s12} and L_{s13} with a lower priority for L_{s23} is considered. The near global optimum solution with the adopted strategy results in a winding configuration as shown in Fig. 6 (a). Control parameters of the respective selected final solution, discriminated by a golden star in Fig. 5 (a), are listed in Table II. Taking a close look at the obtained configuration shows that the distance of the winding from the middle-core limb is minimized which resembles the minimum magnetic length given in equation (19) or windings with minimum mean-turn-length. The second point is the maximum

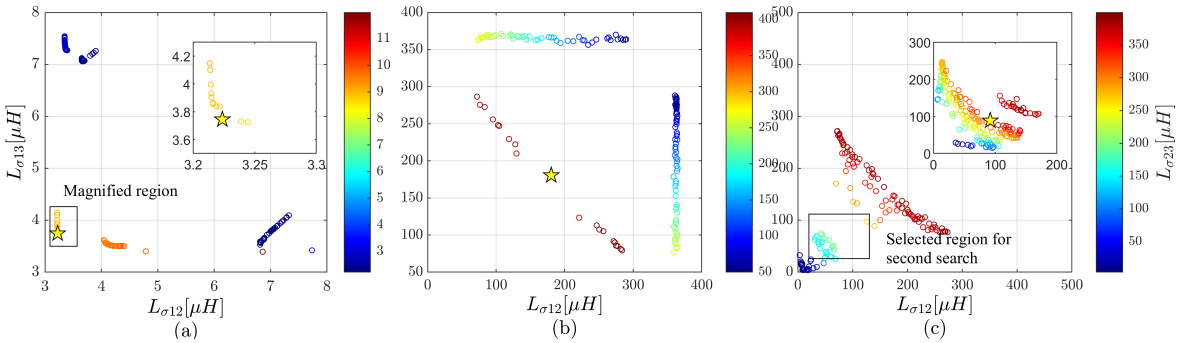

Fig. 5. Pareto optimal solutions from GA: (a) minimizing J_1, (b) minimizing J_2 and (c) minimizing J_3.

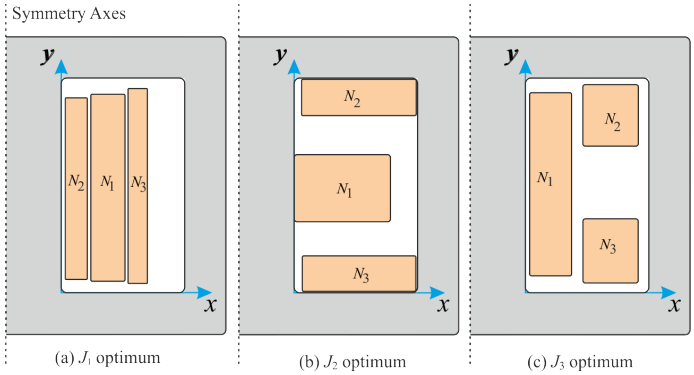

Fig. 6. Optimum winding topologies for: (a) minimizing J_1, (b) minimizing J_2 and (c) minimizing J_3.

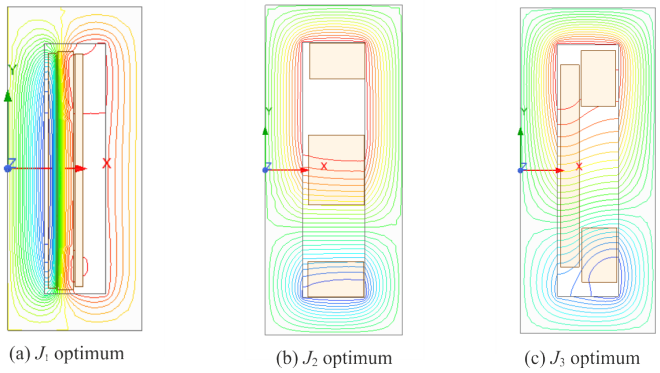

Fig. 7. FEM based short-circuit results for measuring $L_{\sigma 12}$ from: (a) J_1, (b) J_2 and (c) J_3.

distance between W_2 and $W3$ by locating W_1 in between of them. This maximizes the stored energy in their leakage field which is compatible with the assumption for selecting this solution. External inductance should be added to this transformer to satisfy the minimum requirements of the power flow. Adding the external inductances to the secondary side results in completely decoupled output ports which is very important in the considered application.

B. J_2 optimization

J_2 target is to maximize leakage inductance in all windings. The obtained Pareto optimal front from NSGA-II are shown in Fig. 5 (b). These solutions result in a sectional winding structure as shown in the Fig. 6 (b). Similar to J_1, selecting the best solution is a trade-off between L_{s12} and L_{s13} versus L_{s23}. Considering equal L_{s12} and L_{s13} for symmetric output ports result in the discriminated solution with golden star in Fig 5 (b). The control parameters and inductance values are given in Table II. The values of L_{s12} and L_{s13} are relatively high, two times larger than the required inductance for converter operation; this is therefore not an interesting solution given the considered TAB specifications. It could be used in specific MFT as in [22] to limit MMC arm short-circuit level. Other high-leakage inductance applications can be found in [23]. From the winding configuration perspective, all windings benefit from the maximum possible magnetic length. In addition, the distance between W_2 and W_3 is

TABLE II
SELECTED OPTIMUM SOLUTION FROM THE PARETO FRONT SOLUTION SET

Parameters	$J_1(u)$ results	$J_2(u)$ results	$J_3(u)$ results
$x_1/x_2/x_3$ [mm]	4.9/1.4/11.4	2.1/1.9/2.6	1.2/9.2/8.9
$y_1/y_2/y_3$ [mm]	1.6/2.1/2.8	31.0/25.1/80.4	10.9/5.2/70.8
$d_1/d_2/d_3$ [mm]	6.0/3.0/3.1	20.5/20.4/20.2	7.0/13.1/12.8
$h_1/h_2/h_3$ [mm]	88.9/87.8/86.8	25.8/13.0/13.1	75.3/20.2/20.7
$A_{w1}/A_{w2}/A_{w3}$ [mm^2]	529.77/264.89/264.89	529.77/264.89/264.89	529.77/264.89/264.89
$L_{\sigma12}/L_{\sigma13}/L_{\sigma23}$ [μH]	3.24/3.72/8.72	180.36/180.48/406.59	91.97/88.31/317.45
$L_{\sigma1}/L_{\sigma2}/L_{\sigma3}$ [μH]	-0.88/4.12/4.60	-22.88/203.24/203.36	-68.59/160.56/156.90
FEM $L_{\sigma12}/L_{\sigma13}/L_{\sigma23}$ [μH]	3.3/3.82/8.91	179.83/180.49/408.21	92.93/89.11/322.23
FEM $L_{\sigma1}/L_{\sigma2}/L_{\sigma3}$ [μH]	-0.89/4.19/4.715	-23.95/203.77/204.43	-70.10/163.03/159.20
Error $L_{\sigma1}/L_{\sigma2}/L_{\sigma3}$ [%]	1.7/1.8/2.4	4.5/0.3/0.5	2.2/1.5/1.4
Error $L_{\sigma12}/L_{\sigma13}/L_{\sigma23}$ [%]	1.8/2.6/2.1	-0.3/0.0/0.4	1.0/0.9/1.5

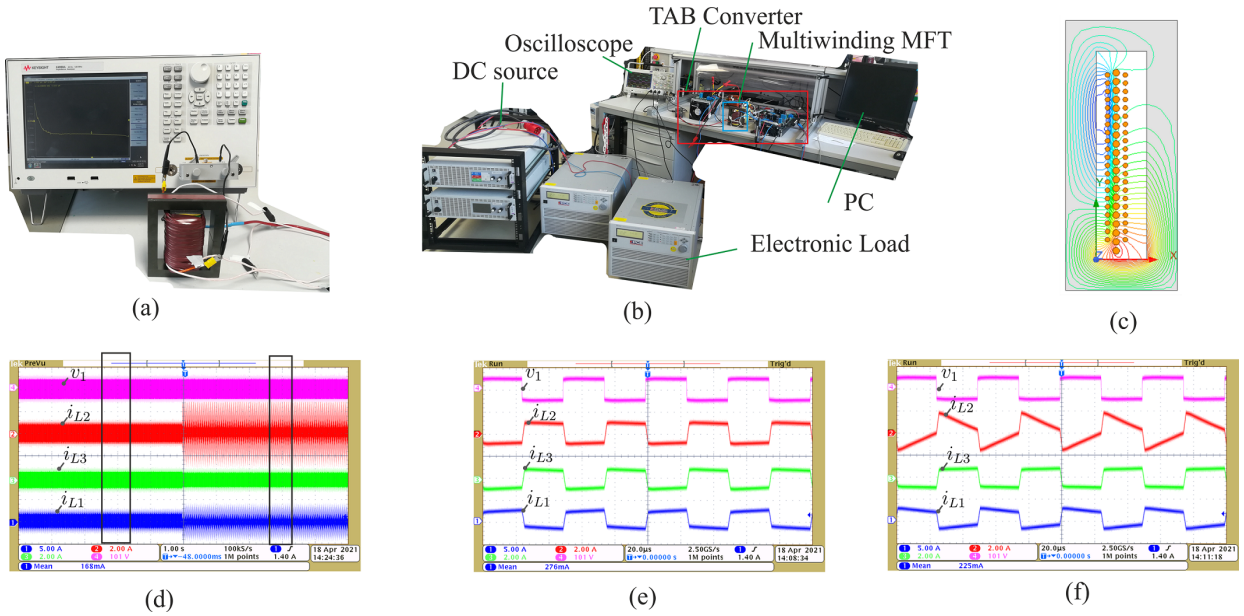

Fig. 8. Experimental results: (a) Characterization of designed transformer with E4990A impedance analyzer, (b) Laboratory set-up, (c) FEM simulation of realized transformer, (d) Overall waveforms with a load step at t=0 in port 2, showing the decoupled behavior. A load step in port 2 does not affect the current characteristics of port 3. (e) Zoomed in waveform before the load step, (f) Zoomed in waveform after the load step

maximum due to the maximized d_i and minimized h_i which stores the maximum energy and achieves a leakage inductance of around 400μH.

C. J_3 optimization

Objective function J_3 is a combination of J_1 and J_2. The stretched Pareto front in Fig. 5 (c) implies on this fact. Due to the broaden Pareto front, selecting the best solution is quite challenging. One criterion in this case could be the required inductances for power flow in the converter. Hence a region of solutions of L_{s12} and L_{s13} in the vicinity of 100μH can be considered as an optimum solution in term of avoiding the external leakage inductances. Therefore a second stage optimization is carried out and the new Pareto optimal and final selected solution are shown in Fig. 5 (c). Corresponding near global optimum winding configuration and numerical values are given in Fig. 6 (c) and Table II respectively. As expected, the achieved optimum winding configuration is a combination of previous two optimum topologies.

D. FEM evaluation

Example designs are validated using FEM simulation in Ansys Maxwell 2D 2021 and eddy currents solution type. The field distribution during short circuits applied from port 1 to port 2 (while port 3 is open circuit) is shown in in Fig.7. The figure shows that the third winding has no impact on the measured leakage inductance as its relative magnetic permeability is similar to air, i.e $\mu_r = 1$. Maximum value of error for all the cases in table II is $|\frac{L_{i,FEM}-L_{i,calc}}{L_{i,FEM}}| \times 100 \leq 5\%$.

V. EXPERIMENTAL VALIDATION

A prototype with three ports has been implemented to test the optimized transformer design. The MFT has been characterized with the E4990A impedance analyzer [Fig. 8 (a)]. The tests have been performed with the specifications provided in Table III and the laboratory set up is depicted in Fig. 8 (b). The feeding port is supplied with a power supply (EA-PSB 9750-40 3U). The two sinking ports are realized with two separated electronic loads, which allow variable load scenarios. Fig. 8 (c)

shows a FEM simulation of the realized transformer. In order to validate the decoupled behavior, the effects of a load change in one load port on the transfer characteristic of the other load port have been investigated. Fig. 8 (d) depicts the overall waveforms. At $t = 0$ the output voltage of port 2 is increased by 30 %. The transformer current through the other load port (i_{L3}) remains almost constant, which validates the decoupled behavior. Fig. 8 (e)-(f) depict the detailed representation of the waveforms of the two operating points.

TABLE III
LABORATORY TEST CONDITIONS.

Parameter	Values
Primary voltage V_1	50 V
Secondary voltage V_{S2}	50 - 70 V
Secondary voltage V_{S3}	50 V
Turns number $\mathrm{n} = \{\mathrm{n}_1, \mathrm{n}_2, \mathrm{n}_3\}$	$\{21, 21, 21\}$
FEM $L_{\sigma 12}/L_{\sigma 13}/L_{\sigma 23}$ [μH]	3.59/4.14/8.31
FEM $L_{\sigma 1}/L_{\sigma 2}/L_{\sigma 3}$ [μH]	-0.29/3.88/4.43
Measurement $L_{\sigma 12}/L_{\sigma 13}/L_{\sigma 23}$ [μH]	4.13/5.43/7.98
Measurement $L_{\sigma 1}/L_{\sigma 2}/L_{\sigma 3}$ [μH]	0.79/3.34/4.46

VI. CONCLUSION

Power flow decoupling of the multiport isolated DC-DC converters is essential where independent operation of the isolated ports is important. Cross-coupling effect in the multiwinding transformers prevents the power flow decoupling in such converters. In this paper, a systematic optimization procedure is introduced to compensate the cross-coupling of the multiwinding medium frequency transformer in the early design stages. Three objective functions are introduced and optimized using multi-objective genetic algorithm (GA). The results are validated by 2D FEM simulations. An experimental prototype is built in the laboratory and connected as the isolation stage of a triple active-bridge (TAB) converter. The results show that the built MFT is capable of minimizing the coupling effects between the TAB ports. Therefore, the cross-coupling between the ports is omitted naturally and the design of the controller is simplified.

REFERENCES

[1] Z. Zheng, Z. Gao, C. Gu, L. Xu, K. Wang, and Y. Li, "Stability and voltage balance control of a modular converter with multiwinding high-frequency transformer," *IEEE transactions on power electronics*, vol. 29, no. 8, pp. 4183–4194, 2013.

[2] C. Gu, Z. Zheng, L. Xu, K. Wang, and Y. Li, "Modeling and control of a multiport power electronic transformer (pet) for electric traction applications," *IEEE Transactions on Power Electronics*, vol. 31, no. 2, pp. 915–927, 2015.

[3] M. R. Islam, Y. Guo, and J. Zhu, "Multiple-input multiple-output medium frequency-link based medium voltage inverter for direct grid connection of photovoltaic arrays," in *2013 International Conference on Electrical Machines and Systems (ICEMS)*. IEEE, 2013, pp. 202–207.

[4] Q. Li, H. Liang, W. Diao, D. Li, and J. Jiang, "Modular battery energy storage system based on one integrated primary multi-secondaries transformer and its independent control strategy," in *2017 IEEE Transportation Electrification Conference and Expo, Asia-Pacific (ITEC Asia-Pacific)*. IEEE, 2017, pp. 1–6.

[5] H. S. Krishnamoorthy, P. Garg, and P. N. Enjeti, "A new medium-voltage energy storage converter topology with medium-frequency transformer isolation," in *2012 IEEE Energy Conversion Congress and Exposition (ECCE)*. IEEE, 2012, pp. 3471–3478.

[6] X. Liu, Z. Zheng, K. Wang, and Y. Li, "An energy router based on multi-winding high-frequency transformer," in *2016 IEEE Applied Power Electronics Conference and Exposition (APEC)*. IEEE, 2016, pp. 3317–3321.

[7] C. Gu, H. Yan, J. Yang, G. Sala, D. De Gaetano, X. Wang, A. Galassini, M. Degano, X. Zhang, and G. Buticchi, "A multiport power conversion system for the more electric aircraft," *IEEE Transactions on Transportation Electrification*, vol. 6, no. 4, pp. 1707–1720, 2020.

[8] C. Gu, Z. Zheng, and Y. Li, "Control strategies of a multiport power electronic transformer (pet) for dc distribution applications," in *2015 IEEE Electric Ship Technologies Symposium (ESTS)*. IEEE, 2015, pp. 135–139.

[9] L. F. Costa, G. Buticchi, and M. Liserre, "Optimum design of a multiple-active-bridge dc–dc converter for smart transformer," *IEEE Transactions on Power Electronics*, vol. 33, no. 12, pp. 10 112–10 121, 2018.

[10] L. F. Costa, F. Hoffmann, G. Buticchi, and M. Liserre, "Comparative analysis of multiple active bridge converters configurations in modular smart transformer," *IEEE Transactions on Industrial Electronics*, vol. 66, no. 1, pp. 191–202, 2018.

[11] C. Zhao, S. D. Round, and J. W. Kolar, "An isolated three-port bidirectional dc-dc converter with decoupled power flow management," *IEEE transactions on power electronics*, vol. 23, no. 5, pp. 2443–2453, 2008.

[12] S. Bandyopadhyay, P. Purgat, Z. Qin, and P. Bauer, "A multiactive bridge converter with inherently decoupled power flows," *IEEE Transactions on Power Electronics*, vol. 36, no. 2, pp. 2231–2245, 2020.

[13] W. G. Hurley and D. J. Wilcox, "Calculation of leakage inductance in transformer windings," *IEEE Transactions on Power electronics*, vol. 9, no. 1, pp. 121–126, 1994.

[14] M. Mogorovic and D. Dujic, "Computationally efficient leakage inductance estimation of multi-winding medium frequency transformers," in *PCIM Europe 2019; International Exhibition and Conference for Power Electronics, Intelligent Motion, Renewable Energy and Energy Management*. VDE, 2019, pp. 1–6.

[15] R. Schlesinger and J. Biela, "Comparison of analytical models of transformer leakage inductance: Accuracy vs. computational effort," *IEEE Transactions on Power Electronics*, 2020.

[16] U. Steiger and S. Mariethoz, "Method to design the leakage inductances of a multiwinding transformer for a multisource energy management system," in *2010 IEEE Vehicle Power and Propulsion Conference*. IEEE, 2010, pp. 1–6.

[17] X. Guo, C. Li, Z. Zheng, and Y. Li, "A general analytical model and optimization for leakage inductances of medium-frequency transformers," *IEEE Journal of Emerging and Selected Topics in Power Electronics*, 2021.

[18] A. Boyajian, "Leakage reactance of irregular distributions of transformer windings by the method of double fourier series [includes discussion]," *Transactions of the American Institute of Electrical Engineers. Part III: Power Apparatus and Systems*, vol. 73, no. 2, pp. 1078–1086, 1954.

[19] K. Deb, A. Pratap, S. Agarwal, and T. Meyarivan, "A fast and elitist multiobjective genetic algorithm: Nsga-ii," *IEEE transactions on evolutionary computation*, vol. 6, no. 2, pp. 182–197, 2002.

[20] C. R. Sullivan and R. Y. Zhang, "Simplified design method for litz wire," in *2014 IEEE Applied Power Electronics Conference and Exposition-APEC 2014*. IEEE, 2014, pp. 2667–2674.

[21] H. Beiranvand, E. Rokrok, and M. Liserre, "Vf-constrained $\eta\rho$-pareto optimisation of medium frequency transformers in isop-dab converters," *IET Power Electronics*, vol. 13, no. 10, pp. 1984–1994, 2020.

[22] G. Zheng, Y. Chen, and Y. Kang, "Modeling and control of the modular multilevel converter (mmc) based solid state transformer (sst) with magnetic integration," *CES Transactions on Electrical Machines and Systems*, vol. 4, no. 4, pp. 309–318, 2020.

[23] J. G. Hayes, N. O'Donovan, M. G. Egan, and T. O'Donnell, "Inductance characterization of high-leakage transformers," in *Eighteenth Annual IEEE Applied Power Electronics Conference and Exposition, 2003. APEC'03.*, vol. 2. IEEE, 2003, pp. 1150–1156.